Shock response and degassing reactions of calcite at planetary impact conditions

Yuhei Umeda (umeda-yuhei@okayama-u.ac.jp)
Okayama University https://orcid.org/0000-0002-9676-6603
Keiya Fukui
Osaka University
Toshimori Sekine
Center for High Pressure Science & Technology Advanced Research
Marco Guarguaglini
https://orcid.org/0000-0002-2660-7543
Alessandra Benuzzi-Mounaix
Ecole Polytechnique
Nobuki Kamimura
Osaka University
Kento Katagiri
Osaka University https://orcid.org/0000-0001-8913-1047
Ryosuke Kodama
Osaka University
Takeshi Matsuoka
Kohei Miyanishi
RIKEN https://orcid.org/0000-0002-6477-3710
Alessandra Ravasio
Ecole Polytechnique https://orcid.org/0000-0002-2077-6493
Takayoshi Sano
Osaka University https://orcid.org/0000-0001-9106-3856
Norimasa Ozaki
Osaka University https://orcid.org/0000-0002-7320-9871

Article

Keywords: Shock response, degassing reactions, calcite, planetary impact conditions, CaCO3

Posted Date: September 21st, 2020

DOI: https://doi.org/10.21203/rs.3.rs-69385/v1

Abstract

Calcite ($CaCO_3$) as a planetary material is a source to the atmospheric carbon dioxide through degassing by high-velocity impact events. Revealing the behavior of calcite in the extreme pressure and temperature conditions is required to understand the impact-induced degassing phenomena. Here we report laboratory investigations of shock- compressed calcite beyond the impact velocity of 12 km/s (faster than escape velocity from the Earth). The present precise shock measurements elucidate the shape of the calcite Hugoniot curve continuously passing through the melting and metallization states up to a pressure of 1000 GPa (= 10-million atmospheres) or a corresponding impact velocity of 30 km/s, allowing us to predict the post-shock residual temperatures and the dominant carbon oxide species in the impact aftermath. These predictions suggest that CO emission is much more dominant than CO2 at the impact velocities of ∼10 km/s and above, affecting the planetary atmospheric chemistry, greenhouse processes, and environmental changes during planetary evolution.

Main Text

Protoplanets formed by repeated collisions of interplanetary dust and asteroids have firstly a primitive atmosphere consisting of mainly hydrogen and helium, called as a “primary” atmosphere. Such an atmosphere was dissipated soon into the outer space by the solar wind due to light molecules. Later, secondary components such as H_2O, CO_2, and N_2 were added into the atmosphere as originated by the degassing of planetary minerals. Carbonate minerals like calcite ($CaCO_3$) are considered to have been the major source of the CO_2 component[1, 2]. The crater chronology of the Moon and the oxygen isotope ratios for zircon indicate that intense meteorite impact events occurred between ∼3.8 and ∼4.1 billion years ago, which is the so-called late heavy bombardment (LHB) period[3, 4]. The impact flux on the Earth during the LHB was at least $\sim 10^3$ times more than that on the present Earth. Moreover, it is believed that collisions exceeding 10 km/s frequently occurred in the LHB period. Therefore, the high-velocity planetary impact-induced degassing of carbonates plays a critical role in the planetary carbon cycle that affects the formation of planetary atmosphere and ocean and the habitability.

Calcite ($CaCO_3$) of carbonates is a typical component in chondritic asteroids[5] and rocky planet surfaces. In fact, the large-scale, catastrophic impact evidence in places abundant in carbonates is visible also on the present Earth as the Chicxulub crater. The shock-compressed calcite behaviors have been investigated only up to 100 GPa pressure, corresponding to an 8 km/s impact velocity. In this study, the Hugoniot pressure-density-temperature (P-ρ-T) relation of calcite was precisely determined to 1000 GPa using the decaying shock method, allowing us to predict the post-impact residual temperatures and the degassed greenhouse gas species.

We performed laser shock experiments on targets illustrated in Fig. 1a and obtained the Hugoniot for calcite shocked between 200 and 1000 GPa (Table S1) using the impedance mismatching technique. Typical images recorded by the velocity interferometer system for any reflector (VISAR) for shock velocity

(U_s) and streak optical pyrometer (SOP) (see Method section) for temperature (T) are shown in Fig. 1b and 1c.

Figure 2a shows the relationship between the shock velocity and the particle velocity (u_p) determined in the present and previous studies. The previous results showed the linear relation; U_s (km/s) = (3.71 ± 0.03) + (1.43 ± 0.01) u_p (km/s)[6] and the extrapolation is in excellent agreement with the SESAME model. The present results are well-approximated also by a linear relation; U_s (km/s) = (3.79 ± 0.33) + (1.26 ± 0.03) u_p (km/s). This linear relation appears to shift downwards parallel to the previous linear extrapolation.

From the present U_s-u_p data, the Hugoniot pressure-density relation was determined through the Hugoniot conservation relations, as shown in Fig. 2b. Our experimental results demonstrate that the SESAME model overestimates shock pressure by more than 100 GPa or density by more than 0.5 g/cc when particle velocity is above ~6 km/s corresponding to ~12 km/s calcite collision velocity. Since the previous experimental data below 100 GPa agree with the SESAME model, the large gap between the present results and the SESAME suggests that any state changes occur with a significant volume change in the 100-200 GPa pressure range.

Figure 3a shows the measured optical reflectivity (R) as a function of the shock pressure. The calcite reflectivity along the decaying shock-velocity history was extracted from the VISAR data. The shock pressure is estimated from the measured shock velocity using the calcite Hugoniot determined in this work. Calcite is found to be reflective over ~200 GPa and the reflectivity steeply increases over ~350 GPa due to the metallization. Similar tendency was observed for shocked quartz and some other insulators.

Figure 3b shows the decaying shock pressure-temperature relationship on calcite, including the previous experimental results[7] and the EOS models[8]. Below ~350 GPa, the obtained Hugoniot P-T curve follows the predicted melting line[9]. The trend of the P-T relationship changes at ~350 GPa, suggesting that the melt completion of calcite along its Hugoniot occurs at ~350 GPa. Above 350 GPa, calcite would be an electronically conducting fluid.

The previous experimental results agree with the SESAME model, but not with the ANEOS and PANDA models. These show that the decomposition reaction of calcite into CaO and CO_2 in the solid phase does not appear in Hugoniot as predicted by the ANEOS and PANDA models at ~80 GPa, because SESAME model does not consider the decomposition reaction. Sekine et al. suggested that the decomposition of shocked $MgCO_3$ occurred at 107 GPa from their recovery experiment results and the Hugoniot and released state measurements[10]. Considering the binding energies of $MgCO_3$ to MgO and CO_2, $CaCO_3$ may decompose at slightly higher shock pressure than $MgCO_3$. Due to the melting and this decomposition reaction, therefore, the previous data points may show a small deviation from the SESAME Hugoniot along the predicted melting line of $CaCO_3$. The Hugoniot P-T data in the previous and present studies can be smoothly connected along the melting line. No optical reflectivity observed below 200 GPa, as shown

in Fig.3a, is consistent with the presumption that the melting and the decomposition reaction dominate in the 100-200 GPa pressure range. Finally, in the pressure range of 100-350 GPa along the melt line, the reactions of melting, decomposition, and dissociation of calcite may sequentially occur.

Implications for natural impacts: carrier of atmospheric components

The adiabatic release paths from Hugoniot state of calcite were calculated using the Mie-Grüneisen equation of state (see Method section) at pressures of 100, 200, and 300 GPa based on our experiments in Fig. 4a (pink, green, and blue diamonds). The Hugoniot temperature T_H and the residual (post-shock) temperature T_R are shown in Figs. 4a and 4b, respectively. After calcite decomposed into CaO and CO_2, the chemical reaction $CO_2 = CO + 1/2O_2$ occurs depending on temperature. The CO/CO_2 ratio produced from calcite shocked at 100, 200, and 300 GPa were estimated to be 6, 10, and 11, respectively, at a total pressure of 1 atm as a function of the residual temperature according to the equilibrium gas-phase diagram[11]. This result shows that the amount of CO generated from $CaCO_3$ increases with increasing shock temperature (shock pressure), because CO is more thermodynamically stable than CO_2 at high temperature.

According to the previous sample recovery experimental results, calcite should be completely degassed at shock pressures above 70 GPa, although there are some variations in the threshold pressure dependent on the starting material of single crystal or powders and capsuled conditions of open or close system (*e.g.*, 10 GPa and 70 GPa by Lange and Ahrens, 1986; at 30-35 GPa and 45 GPa by Martinez et al., 1995; at 20 GPa and 33 GPa by Ohno et al., 2008, respectively[12, 13, 14]). The numerical simulations of the Chicxulub impact reported the total gas amount by the shock-induced volatilization as $(0.8–7.6) \times 10^{16}$ mol[15, 16]. If the CO/CO_2 ratio from shocked calcite is ~10 at an impact pressure of 200 GPa (in a case of our results), the amounts of CO and CO_2 gases produced by the impact become $(0.7–6.9) \times 10^{16}$ mol and $(0.1–0.7) \times 10^{16}$ mol, respectively. According to the previous studies using a light-gas gun, the CO/CO_2 from single crystal calcite shocked at peak shock pressures of below ~100 GPa was estimated to be about 0.1[17]. The residual temperature of the present study was much higher than those of the previous studies. Kawaragi et al. (2009) reported that a CO dominant gas ($CO/CO_2 = 2.02$) increased ~3 K in temperature compared with that in case of only CO_2 in the Chicxulub impact event[18, 19]. CO is known to produce CH_4 and tropospheric O_3 with the strong greenhouse effect through photochemical reactions and has more intense indirect-radiative-forcing to the heat uptake than CO_2[20]. Our results suggest that the indirect greenhouse effect of CO should be taken into account in considering the climate change after the high-speed planetary impact events.

Figure 4b shows that CO/CO_2 ratio in released gas from calcite and the residual temperature as a function of impact pressure. The collision velocity required to generate shock pressures of 100-300 GPa was calculated to be 7-14 km/s for ordinary chondrites[21]. These velocities are typical in planetary impacts[22]. The results suggest the CO gas was produced more significantly in large-scale planetary

impacts than the previously estimated. In natural impacts, CO production proceeds more efficiently than our experimental conditions, since meteorites should relatively increase temperature due to certain amounts of porosity[23]. Especially, it is possible that more CO than expected had been supplied on the Earth by planetary impacts during the LHB period.

Our results may prompt a reconsidering of whole planetary evolution processes on the planetary surface, especially the estimation of the atmospheric compositions and the greenhouse effect, and the seawater temperature. Furthermore, a large amount of CO generated from impacted carbonate rocks may contribute to model the global warming, the planetary atmosphere chemistry, and the biological mass extinction[24] on the Earth triggered by bolide impacts.

Declarations

Acknowledgements

Laser-shock experiments were conducted under the joint research project of the Institute of Laser Engineering, Osaka University. The authors thank Y. Kimura for her support with target fabrication. This work was supported by grants from MEXT Quantum Leap Flagship Program (MEXT Q-LEAP) grant no. JPMXS0118067246, Japan Society for the Promotion of Science (JSPS) KAKENHI (grant nos. 19K21866 and 16H02246), and Genesis Research Institute, Inc. (Konpon-ken, Toyota).

Author contributions

Y.U., K.F. and N.O. conceived the project. Y.U. and K.F. designed and manufactured the targets. Y.U., K.F., T.S., M.G., N.K., K.K., R.K., T.M., K.M., T.S. and N.O. conducted the experiments. Y.U., K.F. and N.K. analyzed the data. Y.U., T.S. and N.O. wrote the manuscript. All authors discussed the results and commented on the manuscript.

Competing financial interests

The authors declare no competing financial interests.

Additional Information

Supplementary information is available for this paper at https://www.nature.com/nastron/

References

1. Grieve, R.A.F., P. B. Robertson, (1979), The terrestrial cratering record 1. Current status of observations. Icarus, 38, 212–229.
2. Hildebrand, A.R., G. T. Penfield, D. A. Kring, M. Pilkington, A. Z. Camargo, S. B. Jacobnsen, W. V. Boynton, (1991), Chicxulub crater: a possible Cretaceous/Tertiary boundaryimpact crater on the Yukatan Peninsula, Mexico. Geology, 19, 867–871.

3. Culler, T. S., T. A., Becker, R. A., Muller, P. R., Renne, (2000), Lunar impact history from 40Ar/39Ar dating of glass spheres. Science, 287, 1785–1788.
4. Valley, J. W., W. H. Peck, E. M. King, and S.A. Wilde, (2002), A cool early Earth. Geology, 30, 351–354.
5. Leuw, S., A. E., Rubin, and J. T., Wasson, (2010), Carbonates in CM chondrites: Complex formational histories and comparison to carbonates in CI chondrites,Meteoritics & Planetary Science,45, 513–530.
6. Kalashnikov, N. G., M. N. Pavlovskiy, G. V. Simakov, and R. F. Trunin, (1973), Dynamic compressibility of calcite-group minerals, Izv. Earth Physics, 2, 23-29.
7. Gupta, S.C., S. G. Love, and T. J. Ahrens, (2002), Shock temperature in calcite ($CaCO_3$) at 95–160 GPa. Earth Planet. Sci. Lett., 201, 1–12.
8. Kerley, G. I., (1989), Equations of state for calcite minerals. I. theoretical model for dry calcium carbonate, High Pressure Research, 2(1), 29–47.
9. Wünnemann, K., G.S. Collins, G.R. Osinski (2008), Numerical modelling of impact melt production in porous rocks, Earth and Planetary Science Letters 269, 530–539.
10. Sekine, T., H. He, T. Kobayashi, and A. Yamaguchi, (2006), Hugoniot and impact-induced phase transition of magnesite. American Mineralogist, 91, 1802–1806.
11. Kress, M. E. and C. P. McKay, (2004), Formation of methane in comet impacts: implications for Earth, Mars, and Titan, Icarus, 168, 475–483.
12. Lange, M. A., and T. J. Ahrens, (1986), Shock-induced CO_2 loss from $CaCO_3$; implications for early planetary atmosphere, Earth Planet. Sci. Lett., 77, 409–418.
13. Martinez, I., A. Deutsch, U. Scha¨rer, P. Ildefonse, F. Guyot, P. Agrinier, (1995), Shock recovery experiments on dolomite and thermodynamical calculations of impact induced decarbonation, J. Geophys. Res., 100, 15465–15476.
14. Ohno, S., T. Kadono, K. Ishibashi, K. Kawaragi, S. Sugita, E. Nakamura, and T. Matsui, (2008), Direct measurements of impact devolatilization of calcite using a laser gun, Geophys. Res. Lett., 35, L13202, http://dx.doi.org/10.1029/2008GL033796.
15. Pope, K.O., K. H. Baines, A. C. Ocampo, and B. A. Ivanov, (1997), Energy, volatile production, and climatic effects of the Chicxulub Cretaceous/Tertiary impact, J. Geophys. Res., 102, 21645–21664.
16. Pierazzo, E., D. A. Kring, and H. J. Melosh, (1998), Hydrocode simulation of the Chicxulub impact event and the production of climatically active gases, J. Geophys. Res., 103, 28607–28625.
17. Kurosawa, K., S. Ohno, S. Sugita, T. Mieno, T. Matsui, and S. Hasegawa, (2012), The nature of shock-induced calcite ($CaCO_3$) devolatilization in an open system investigated using a two-stage light gas gun, Earth Planet. Sci. Lett., 337–338, 68–76.
18. Kawaragi, K., Y. Sekine, T. Kadono, S. Sugita, S. Ohno, K. Ishibashi, K. Kurosawa, T. Matsui, S. Ikeda, (2009), Direct measurements of chemical composition of shock-induced gases from calcite: an intense global warming after the Chixulub impact due to the indirect greenhouse effect of carbon monoxide, Earth Planet. Sci. Lett., 282, 56–64.

19. Gulick, S.P.S., P. J. Barton, G. L. Christeson, J. V. Morgan, M. McDonald, K. M. Cervantes, Z. F. Pearson, A. Surendra, J. U. Fucugauchi, P. M. Vermeesch, and M. R. Warner, (2008), Importance of pre-impact crustal structure for the asymmetry of the Chicxulub impact crater. Nat. Geosci., 1, 131–135.
20. Daniel, J.S., and S. Solomon, (1998), On the climate forcing of carbon monoxide. J. Geophys. Res. 103, 13249–13260.
21. Zhang, F., and T. Sekine, (2007), Impact-shock behavior of Mg- and Ca-sulfates and their hydrates, Geochim. Cosmochim. Acta., 71, 4125.
22. Arakawa, M., M. Yasui, and Y. Shimaki, (2014), High-Velocity Impact Phenomena in the Solar System Related to the Origin and Evolution of Planets, Review of High Pressure Science and Technology, 24(1), 13–20.
23. Bischoff, A., M. Horstmann, A. Pack, M. Laubenstein, and S. Haberer, (2010), Asteroid 2008 TC3—Almahata Sitta: A spectacular breccia containing many different ureilitic and chondritic lithologies. Meteoritics & Planetary Science, 45(10-11), 1638-1656.
24. Ohno, S., T. Kadono, K. Kurosawa, T. Hamura, T. Sakaiya, K. Shigemori, Y. Hironaka, T. Sano, T. Warari, K. Otani, T. Matsui, and S. Sugita, (2014), Production of sulphate-rich vapour during the Chicxulub impact and implications for ocean acidification. Nature Geoscience, *7*(4), 279-282.
25. Sekine, T., et al. (2016), Shock compression response of forsterite above 250 GPa, Sci. Adv., 2, e1600157, doi:10.1126/sciadv.1600157.
26. Bolis, R. M., et al., (2016), Decaying shock studies of phase transitions in MgO-SiO_2 systems: Implications for the super-Earths' interiors. Geophysical Research Letters, 43(18), 9475–9483.
27. Barker, L. M., and R. E. Hollenbach, (1972), Laser interferometer for measuring high velocities of any reflecting surface, J. Appl. Phys., 43, 4669–4775.
28. Miller, J. E., T. R. Boehly, A. Melchior, D. D. Meyerhofer, P. M. Celliers, J. Eggert, D. G. Hicks, C. M. Sorce, J. A. Oertel, and P. M. Emmel, (2007), Streaked optical pyrometer system for laser-driven shock-wave experiments on OMEGA. Review of Scientific Instruments, 78(3), 034903.
29. Hicks, D. G., T. R. Boehly, J. H. Eggert, J. E. Miller, P. M. Celliers, and G. W. Collins (2006), Dissociation of liquid silica at high pressures and temperatures, Phys. Rev. Lett., 97(2), 3–6, doi:10.1103/PhysRevLett.97.025502.
30. Celliers, P. M., G.W. Collins, D. G. Hicks, and J. H. Eggert (2005), Systematic uncertainties in shock-wave impedance-match analysis and the high- pressure equation of state of Al, J. Appl. Phys., 98, 113529.
31. Knudson, M. D., R. W. Lemke, D. B. Hayes, C. A. Hall, C. Deeney, and J. R. Asay (2003), Near-absolute Hugoniot measurements in aluminum to 500 GPa using a magnetically accelerated flyer plate technique, Journal of Applied Physics, 94, 4420, doi: 10.1063/1.1604967.
32. Knudson, M. D., and M. P. Desjarlais, (2009), Shock Compression of Quartz to 1.6 TPa: Redefining a Pressure Standard, Phys. Rev. Lett., 1003, 225501, doi: 10.1103/PhysRevLett.103.225501.

33. Zeldovich, Y. B., and Y. P. Raizer (1967), Physics of Shock Waves and High-Temperature Hydrodynamic Phenomena, Academic, New York.
34. Eggert, J., S. Brygoo, P. Loubeyre, R. S. McWilliams, P. M. Celliers, D. G. Hicks, T. R. Boehly, R. Jeanloz, and G. W. Collins, (2008), Hugoniot Data for Helium in the Ionization Regime, Phys. Rev. Lett. 100, 124503.
35. Celliers, P. M., P. Loubeyre, J.H. Eggert, S. Brygoo, R.S. McWilliams, D.G. Hicks, T.R. Boehly, R. Jeanloz, and G.W. Collins (2010). Insulator-to-conducting transition in dense fluid helium. Physical Review Letters, 104(18), 184503.
36. Millot, M., N. A. Dubrovinskaia, A. Cernok, S. Blaha, L. S. Dubrovinsky, D. G. Braun, P. M. Celliers, G. W. Collins, J. H. Eggert, and R. Jeanloz, (2015), Shock compression of stishovite and melting of silica at planetary interior conditions, Science, 347(6220), 418, doi:10.1126/ science.1261507.
37. Knudson, M. D., and M. P. Desjarlais, (2013), Adiabatic release measurements in α-quartz between 300 and 1200 GPa: Characterization of α-quartz as a shock standard in the multimegabar regime, Physical Review B, 88, 184107.
38. Anderson, O. L., (2000), The Grüneisen ratio for the last 30 years, Geophys. J. Int., 143, 279–294.
39. Raikes, S. A., and T. J. Ahrens, (1979), Post-shock temperatures in minerals, Geophys. J. R. astr. Soc., 58, 717–747.

Materials And Methods

Hugoniot and temperature data of calcite

The Hugoniot relations on calcite have been determined experimentally at pressure below 95 GPa[6]. On the other hand, only the theoretical model (SESAME 7331) is available at pressures above 200 GPa, and there are some data on the U_s-u_p relations from the calculation models (SESAME, ANEOS, and PANDA[8, 16]). Thus, we require experimental data above 100 GPa to understand the dynamic behaviors in natural impacts. Extreme pressure and temperature conditions over 200 GPa and 5000 K will be generated at impact velocities of chondritic meteorites over 10 km/s using the Hugoniot relations [21, 25, 26].

The shock temperature on calcite was measured up to a pressure of 160 GPa in the previous study using gas gun[7]. Temperature data of shocked calcite above 200 GPa are required to understand the reactions on calcite. Extrapolations of the temperature calculations by the ANEOS and PANDA models showed high temperatures relative to the SESAME data at high pressure over ~100 GPa. For example, the temperatures at 300 GPa by the ANEOS and the PANDA models are 8000 K and 3000 K lower than that by the SESAME model, respectively.

Laser shock experiments and optical measurements of pressure and temperature

The laser shock experiments on calcite were conducted with GEKKO XII laser facility at Osaka University. The GEKKO facility is a neodymium-doped glass laser (the basic wavelength: ω 1053 nm) system. The

total 12 beams of three 2ω beams with a diameter of 1000 μm and nine 3ω beams with a diameter of 600 μm were used in this experiment. The temporal shape of the laser pulse was approximately square with a 2.5 ns duration [full width at half-maximum (FWHM)] and rise and fall times of 100 ps each. The total energy and intensity of laser were 300–800 J and 10^{12}–10^{13} W/cm^2 on the target in the present study, respectively.

We used ~1 cm natural single crystals of calcite $CaCO_3$ (density: 2.71 g/cm^3). The crystals were polished to be 4 mm square plates (500 μm thick) by a manufacture. The target assemblage used in the present study is shown in Fig. 1a. All materials of the target were glued with an ultraviolet curing resin. Typical resin was ~1 μm thick.

Shock velocity and the thermal emission at the shock wave front of samples were measured by using the Velocity Interferometer System for Any Reflector (VISAR)[27] and Streak Optical Pyrometer (SOP)[28], respectively. As quartz becomes a high optical reflectance above 150 GPa[29], we can measure the shock velocity. And if calcite becomes reflective at high shock pressure, we can measure both shock velocities on the target simultaneously. Although refractive index of a crystal varies with the crystal orientation, the refractive index used in the present study is 1.66 and 1.55 for calcite and quartz, respectively. Velocity sensitivities [velocity per fringe (VPF)] of two line-imaging VISARs (line-VISARs) in this study were 7.39 and 4.47 km/s in vacuum. Based on the quartz U_s measured by VISAR, the pressure (P), particle velocity (u_p), and U_s for Al were obtained by the impedance matching for the interface between Al and quartz. The experimental error of a shock velocity was less than 5 % of the velocity sensitivities.

After that, the u_p of calcite was determined by the impedance mismatching method[30] for the interface between Al and calcite. The U_s (km/s) -u_p (km/s) relations used for quartz and Al are $U_s = (6.26 \pm 0.35) + (1.20 \mp 0.02)\ u_p - (2.56 \mp 0.15)\ u_p \exp[-(0.37 \pm 0.02)\ u_p]$ and $U_s = (6.375 \pm 0.25) + (1.18 \pm 0.03)\ u_p$, respectively[31, 32]. Shock pressure and density (ρ) in calcite were determined from the U_s and u_p using the basic conservation relations[33]. Uncertainties in impedance mismatching method were propagated through a Monte Carlo method[34], hence one-sigma uncertainties were taken to be standard deviation of the distributions. In addition, the reflectivity of shocked calcite was simultaneously obtained from VISAR measurements at the probe laser (532 nm). The reflectivity of shocked quartz was cited from a reference[35].

The SOP measures the thermal emission from the shock around a 455-nm wavelength with a narrow bandwidth (38-nm FWHM). The brightness temperature is determined using the gray-body Planck spectrum:

$$L(\lambda, T) = \varepsilon \frac{2hc^2}{\lambda^5}\left(e^{\frac{hc}{\lambda k_B T}} - 1\right)^{-1} \qquad (1)$$

where h is Planck's constant, c is the speed of light, λ is the wavelength of the radiation, T is the temperature of the Planckian source, K_B is the Boltzmann constant, and ε is the emissivity of the shocked matter. This equation can be reduced to a practical form at the narrow band wavelengths[28], as described by Miller et al. (2007).

$$T = \frac{T_0}{\ln\left(\frac{A\varepsilon}{C}+1\right)} \qquad (2)$$

where T_0 and A are calibration parameters that depend on the SOP optical system and C is the CCD (charge-coupled device) counts obtained by the streak camera system. The emissivity ε is calculated from the Kirchhoff law, $\varepsilon = 1 - R$, where R is the shock-front reflectivity. We used quartz as the standard material because the relations between T-U_s and R-U_s have been precisely measured[29, 36]. We determined the value of A from several calibration shots on quartz to measure U_s and SOP simultaneously. More details of the SOP measurement can be found in the previous studies[25, 26].

Estimation of an adiabatic release state

The adiabatic release state of shocked calcite was determined to estimate the residual temperature at pressure release. Release isentrope was approximated by using Mie-Grüneisen equation of state[37]. At first, the following Eq. (1) was given by combining the Rankine-Hugoniot equations with Mie-Grüneisen EOS

$$P_S(V) = P_H(V)\left[1 - \frac{\Gamma}{2V}(V_0 - V)\right] + \frac{\Gamma}{V}[E_S(V) - E_0] \qquad (1)$$

where P, E and V are the pressure, internal energy and the specific volume, respectively. Grüneisen parameter Γ was assumed to be a function of V only, using $\Gamma_0 = 0.57$[38],

$$\Gamma = \Gamma_0 \frac{V}{V_0} \qquad (2)$$

The subscript H, S, and 0 denote the reference Hugoniot, release adiabat, and the initial state, respectively. The internal energy on an isentrope was determined by solving the ordinary differential equation (ODE), which gives

$$E_s - E_0 = \exp\left[\frac{\Gamma_0}{V_0}(V_1 - V)\right]\left\{\frac{P_1(V_0 - V_1)}{2} - \int_{V_1}^{V} P_H\left[1 - \frac{\Gamma_0}{2V_0}(V_0 - V')\right] \times \exp\left[\frac{\Gamma_0}{V_0}(V' - V_1)\right] dV'\right\} \qquad (3)$$

where subscript 1 refers to shocked state. Substituting Eq. (3) into Eq. (1), we determined the adiabatic release state of calcite using the measured P_1, V_1, and the obtained calcite Hugoniot.

The residual (post-shock) temperature T_R was given by Eq. (4)[39]

$$T_R = T_1 \exp\left(\int_{V_1}^{V_2} \frac{\Gamma(V')}{V'} dV'\right) \quad (4)$$

where T_1 and V_2 denote the initial shocked temperature and residual specific volume, respectively.

Figures

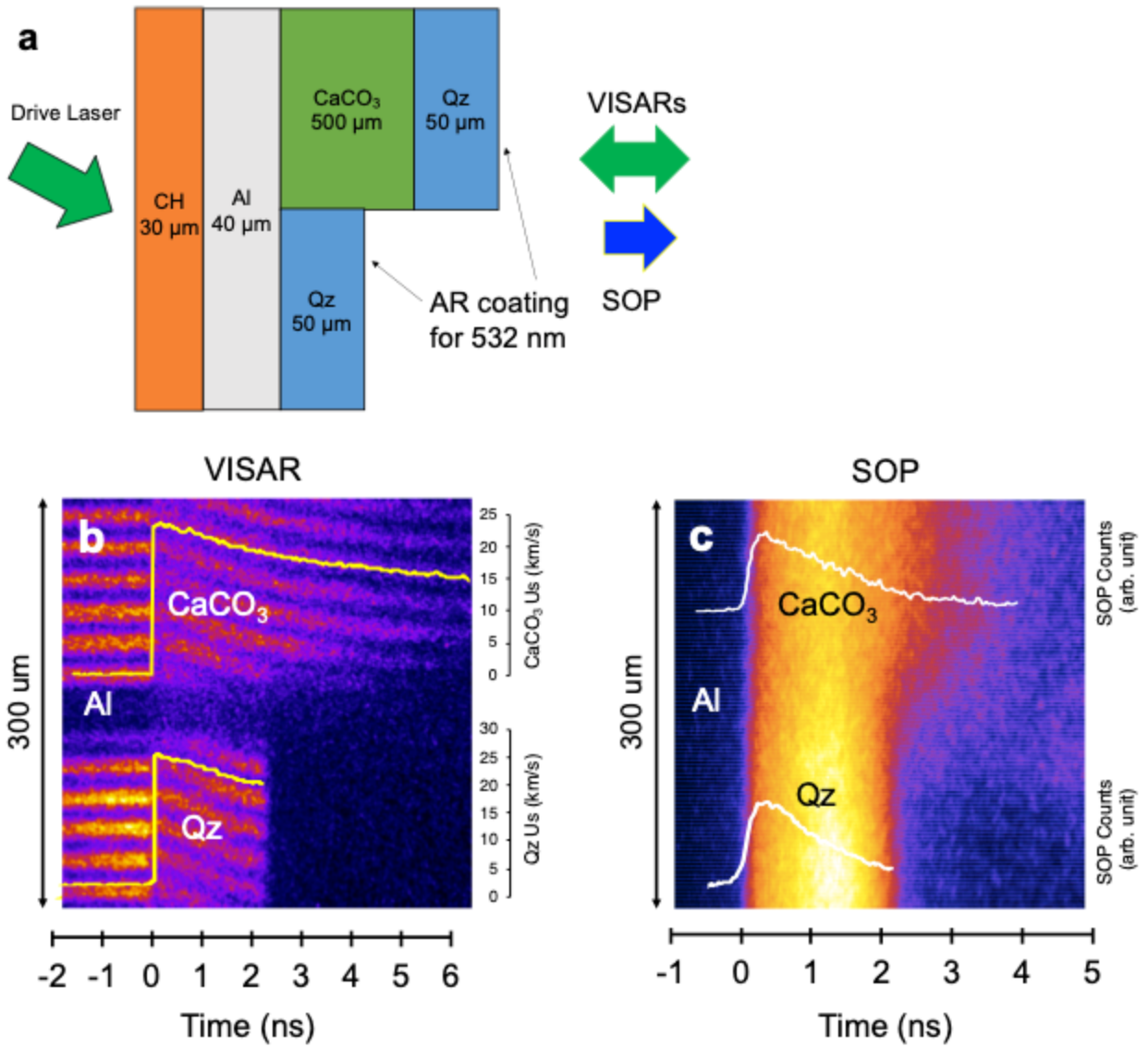

Figure 1

Schematic setup and typical measurements by VISAR and SOP in laser shock experiments. a, The target assembly consisted of poly-propylene (CH), aluminum (Al), crystalline α-quartz (Qz), and calcite (CaCO3) from the drive laser side (GEKKO XII). The thickness was 30, 40, 50, and 500 μm for CH, Al, SiO2, and CaCO3, respectively. The CH was used as an ablator to generate a shock wave, and Al as the base plate, and SiO2 as the reference material for the impedance mismatching analysis and the temperature determination. The VISAR side of SiO2 was coated with an anti-reflected (AR) layer for a probe laser at the wavelength of 532 nm. Since AR coating could not be available for calcite and SiO2 has almost the same refractive index with calcite., the last SiO2 after calcite was used for the window material. b and c, VISAR line-imaging velocity record and inferred shock velocity (yellow curve, scale on right). Corresponding SOP raw image and count profiles considering the emissivity (1-R) (white curve). The time zero is set to the arrival time of shock wave on the Al/CaCO3 and Al/Qz interfaces. The vertical width in images is about 300 μm.

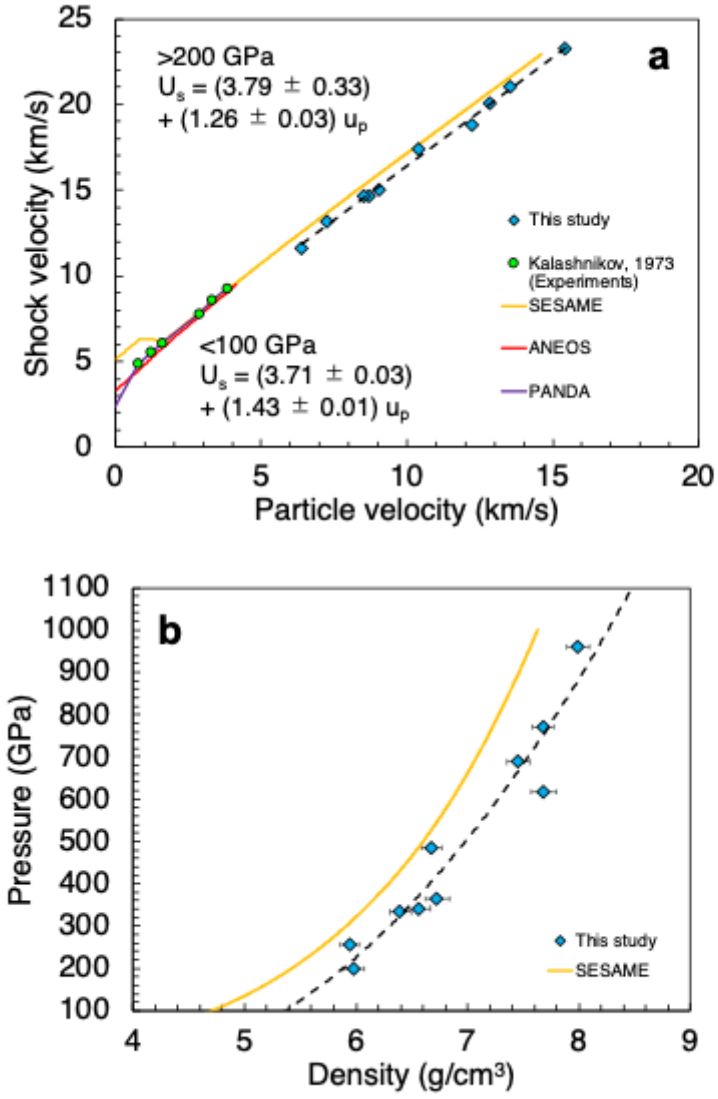

Figure 2

Hugoniot relations of calcite. a, The Us-up data of this study are shown as light blue diamonds and connected linearly as the broken line. The error bars of this study are smaller than the symbol size. The open green circles indicate the experimental result 6 by Kalashnikov, (1973). The orange, red, and purple solid lines represent SESAME, ANEOS, and PANDA models, respectively 8, 16. b, The pressure-density data determined in this study are shown as light blue diamonds and connected by the broken curve, and compared with the SESAME model as orange solid curve.

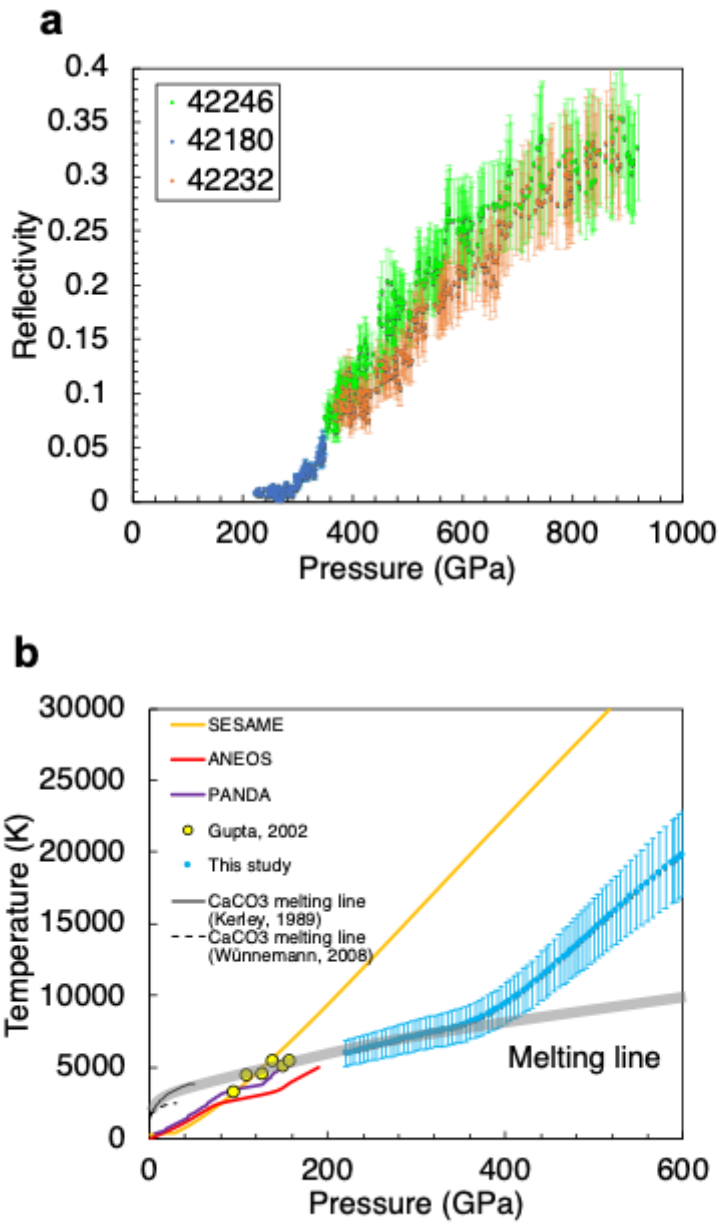

Figure 3

The reflectivity at 532 nm and the temperature as a function of pressure. a, The green, blue, and orange plots are shots 42246, 42180, and 42232, respectively. b, The light blue plots indicates our result from the decaying shock experiment. The orange, red, and purple solid lines represent SESAME, ANEOS, and PANDA models, respectively 8, 16. The open yellow circles indicate the experimental results 7. The solid

and dotted black line mean the calcite melt lines at low pressures 8, 9. The grey bold line indicates the calcite melting line proposed by this study.

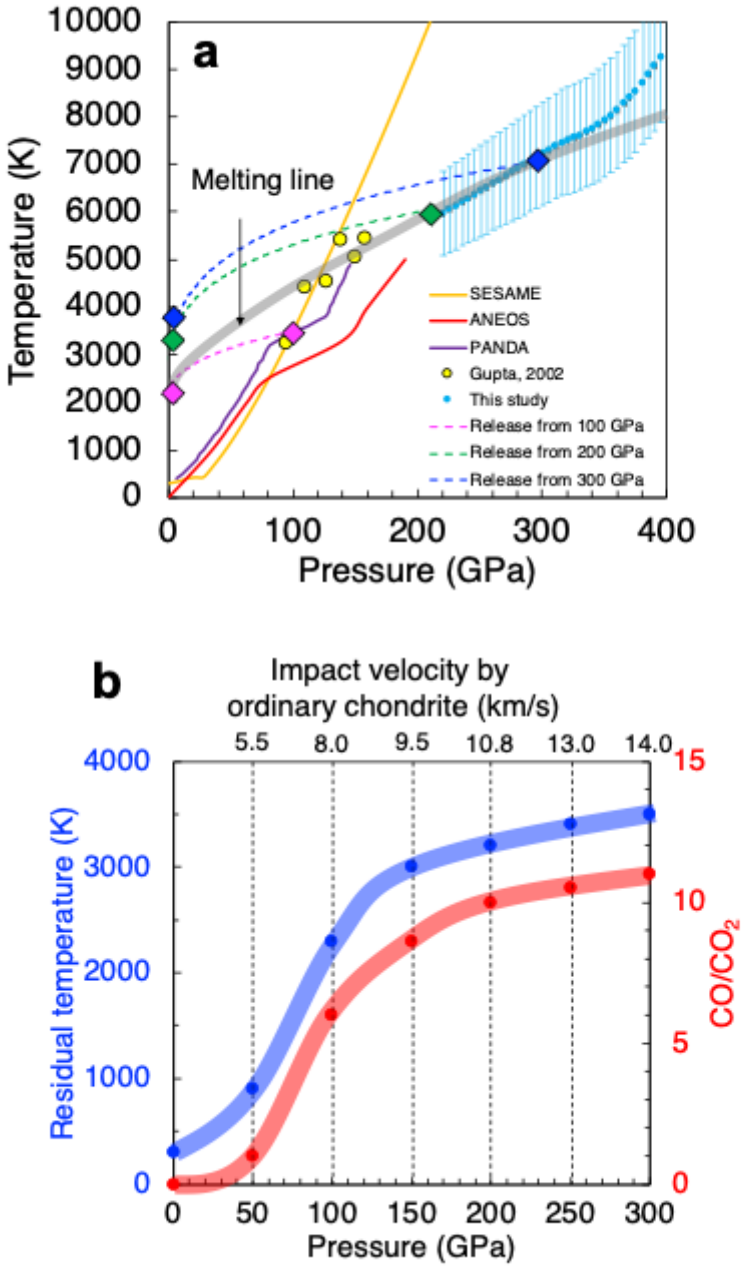

Figure 4

The release isentrope and the residual temperature and the CO/CO2 ratio of shocked calcite as a function of pressure (impact velocity). a, The release isentrope paths (dotted lines) of shocked calcite from 100, 200, and 300 GPa in the magnification of Fig. 3b. The diamonds of pink, green, and blue mean the start and the end points of releasing. b, The residual temperature (blue; left axis) and the CO/CO2 ratio (red; right axis) as a function of pressure. The impact velocity was calculated using the Us-up for the ordinary

chondrite 21 proposed from Zhang and Sekine, (2007) at the vertical impact. The CO/CO2 ratio was estimated using the equilibrium gas-phase diagram as a function of temperature 11.

Supplementary Files

This is a list of supplementary files associated with this preprint. Click to download.

- v2NatComEarthUmedacalciteSM.docx